New insights into the role of MWCNT in cement hydration

Meng, Shaoqiang; Ouyang, Xiaowei; Fu, Jiyang; Ma, Yuwei; Ye, Guang

DOI
10.1617/s11527-021-01832-5

Publication date
2021

Document Version
Final published version

Published in
Materials and Structures/Materiaux et Constructions

Materials and Structures (2021) 54:238
https://doi.org/10.1617/s11527-021-01832-5

ORIGINAL ARTICLE

New insights into the role of MWCNT in cement hydration

Shaoqiang Meng · Xiaowei Ouyang · Jiyang Fu · Yuwei Ma · Guang Ye

Received: 22 September 2021 / Accepted: 24 November 2021

Abstract Investigating the mechanism of multi-walled carbon nanotube (MWCNT) in the early cement hydration enables better utilization of the potential of MWCNT as reinforcing agents in cement composites. The interaction of MWCNT with ions and its effect on cement hydration were investigated. Zeta potential measurement was intended to discuss the interaction of the MWCNT surface with Ca^{2+}. Then, the formation processes of C–S–H were observed with a scanning electron microscope (SEM). The influence of MWCNT on the early cement hydration was investigated using isothermal calorimetry. The results showed that MWCNT significantly accelerates early cement hydration. It is likely attributed to its high surface area and strong adsorption for Ca^{2+}, which greatly promotes the migration of ions, especially Ca^{2+}, and thus the precipitation of ions on the cement surface. This facilitates the C–S–H nucleation and growth process, thus the cement hydration. These results also indicated that the MWCNT would not provide a stable nucleation site for C–S–H, since the size of MWCNT is less than that of C–S–H.

Keywords MWCNT · Cement paste · Hydration · C–S–H · Nucleation · Calcium ion

1 Introduction

With the progress of nanotechnology, many studies [4, 18, 34, 44] were carried out on the use of nanomaterials in cement-based materials, e.g., graphene, graphene oxide, multi-walled carbon nanotube (MWCNT), nano-silica, nano-TiO2. MWCNT showed great potential as a reinforcing additive for cement-based materials due to its high modulus of elasticity, high tensile strength, and prime conductivity [36]. Reinforcement of cement-based materials with MWCNT can provide a new pathway for improving the properties (e.g., mechanical properties, electromagnetic properties, and durability) of building materials, and thus the engineering structures.

Many studies [3, 11, 39] have shown that MWCNT can increase the strength, toughness, and permeability resistance of cement-based materials. Calixto et al. [37] found that 0.15wt% MWCNT increased the compressive strength of the cement paste by 28%. Mahdi et al. [17] found that incorporation of carboxyl-functionalized MWCNT into cement mortars increased the compressive strength by 39%. An

S. Meng · X. Ouyang (✉) · J. Fu · Y. Ma
Research Center for Wind Engineering and Engineering Vibration, Guangzhou University, Guangzhou 510006, China
e-mail: xwouyang@gzhu.edu.cn

G. Ye
Department of Materials and Environment (Microlab), Faculty of Civil Engineering and Geosciences, Delft University of Technology, 2628CN Delft, The Netherlands

Published online: 02 December 2021

increase in electrical conductivity was also reported in cement paste containing MWCNT [1, 2, 22]. Maria et al. [8, 12] reported that MWCNT can reduce the capillary stress of cement paste and improve its durability. Li et al. [43] showed that the addition of 0.10wt% of MWCNT enhanced the average initial cracking fracture toughness by about 21%.

The macroscopic properties of cement-based materials are determined by their microscopic characteristics. Many studies [9, 10, 33] have concluded that MWCNT-modified cement-based materials have lower porosity and denser microstructure due to the promotion of hydration products by MWCNT. As the main hydration product, C-S–H plays an important role in the microscopic properties of cement-based materials [29]. However, few studies of the effect of MWCNT on C-S–H have been reported. Wang et al. [42] showed that the addition of MWCNT results in the decrease of $Ca(OH)_2$ and hydration promotion. In addition, MWCNT enhanced the chemical bond strength of the groups between Ca, O, and Si atoms in the C–S–H gels, thus contributing to the degree of polymerization. Makar et al. [16] also reported that single-walled carbon nanotubes promote the generation of C–S–H and that these C–S–H are preferentially generated around single-walled carbon nanotubes. Petrunin et al. [31] suggested that the oxygen-containing functional groups of MWCNT caused the increase of the concentration of C–S–H from 65.9% to 74.4%. Li et al. [15] demonstrated that the addition of 0.1% functionalized MWCNT led to a finer C–S–H and a more compact microstructure. These studies attribute the promotion of the cement hydration process to the 'nucleation effect' of MWCNT. Conversely, some researchers [5, 14, 35, 38] affirmed that MWCNT has no 'nucleation effect'. Therefore, the mechanism of the effect of MWCNT on the early cement hydration needs to be further verified.

The nucleation and growth of C–S–H play a key role in the early cement hydration [6]. Two processes of the formation of C–S–H have generally been known: the nucleation process and the nucleation growth process [7]. In the pore solution of cement paste, ions are always in a constant state of motion. These ions are adsorbed to form ion clusters on the matrix surface. There are interaction forces between ion clusters and ions. When the ion concentration is saturated, these clusters become large and then form nuclei, which gradually enter the growth process. Our previous studies [19] have found that graphene and graphene oxide promotes the nucleation and growth of C–S–H by affecting the migration of ions (especially Ca^{2+}) in cement solutions. MWCNT, which has excellent electrical conductivity, can accelerate the migration of ions in the solution [28]. It is necessary to study the effect of MWCNT interaction with ions on cement hydration. The effect of MWCNT on cement hydration is analyzed from the perspective of ionic interaction, which provides a deep understanding of the action of MWCNT in the nucleation and growth process of C–S–H.

Ca^{2+} is closely related to the kinetic, morphological, and structural characteristics of C–S–H [6]. For this research, the interaction of MWCNT with Ca^{2+} was characterized and the nucleation and growth processes of C–S–H on the cement surface were observed by SEM. Then, isothermal calorimetry was applied to provide some information about hydration kinetics up to 24 h after mixing. Based on these tests, the mechanism of the effect of MWCNT on the early cement hydration was discussed.

2 Materials

2.1 Materials and mixture

In this study, the cement used was Portland cement type I and the chemical compositions obtained by X-ray fluorescence (XRF) analysis are listed in Table 1. The specific physical parameters of MWCNT are demonstrated in Table 2. The morphology of MWCNT was observed by SEM, as presented in Fig. 1. The mixing proportions are reported in Table 3. Two series of samples were prepared and named PC and CC. PC was a cement paste without MWCNT. CC was a cement paste with MWCNT. The content of MWCNT was 0.4% by weight of cement.

2.2 Sample preparation

The fresh paste was prepared as following processes: First, MWCNT and water were mixed to get a stable MWCNT suspension. The MWCNT suspension was sonicated for 15 min using an ultrasonic meter. Then, adding cement into the MWCNT suspension and stirred for 1 min at low speed and 1 min at high speed. Afterward, the samples were cured at a

Table 1 Chemical compositions of cement (wt%)

CaO	SiO_2	Al_2O_3	Fe_2O_3	SO_3	MgO	K_2O	TiO_2	P_2O_5	Na_2O
63.29	21.32	5.46	3.46	2.31	1.79	0.632	0.513	0.342	0.287

Table 2 Physical parameters of MWCNT

Purity wt%	Inner diameter nm	Outer diameter nm	Length μm	Specific surface area m^2/g	Density g/cm^3	Resistivity μΩm
> 95	3–5	8–15	3–12	> 233	0.15	1412

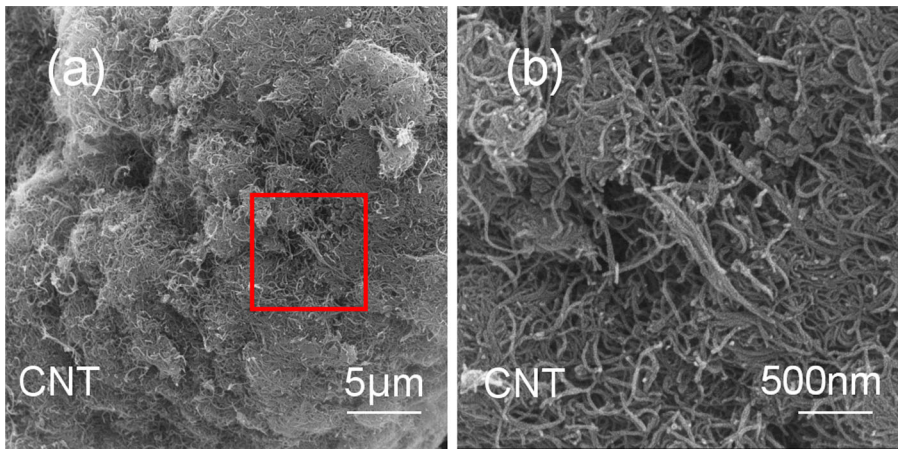

Fig. 1 SEM image of MWCNT (**a**) and local enlarged (**b**)

Table 3 Mix compositions of cement pastes

Name	Cement (wt%)	MWCNT (wt%)	w/b
PC	100	0	0.4
CC	100	0.4	0.4

temperature of 20 ± 1 °C n 99% relative humidity for specific times (15 min, 1, 4, and 7 h). When reaching requires hydration time, about 1 g of the sample was terminated hydration by immersion in anhydrous alcohol. Finally, the specimens were stored in a vacuum desiccator until used.

2.3 Zeta potential test

The surface charge properties of the particle can be characterized by a zeta potential test [24]. Figure 2 shows the schematic of the zeta potential test. Charged particles were attracted to counter-ions in solution. These anti-number ions form a two-electron layer structure: the stern layer and the diffuse layer [32]. Within the diffusion layer, there was a shear plane and the zeta potential refers to the potential at the position of the shear plane, which reflects the interactions of ions with the surface. These interactions on the particle surface affect the process of heterogeneous nucleation and growth of mineral phases on its surface [7].

Zeta potential was tested by Malvern Zetasizer Nano from Malvern Instruments Ltd., UK. Zeta potential reflects the interaction of Ca^{2+} with the particle, which significantly affects the nucleation and growth of hydration products [24]. The zeta potential was measured by suspending MWCNT particles in simulated solutions with different concentrations of

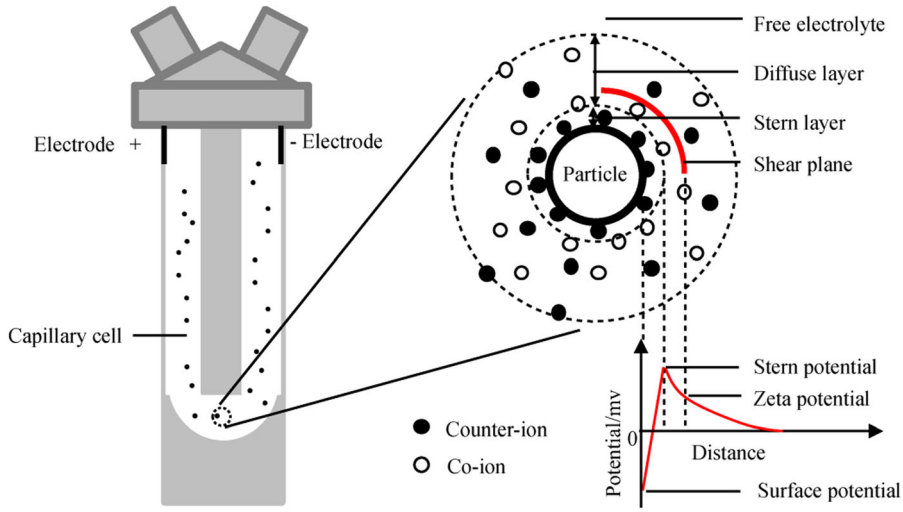

Fig. 2 Schematic illustration of the electrical double layer and zeta potential [24]

$Ca(OH)_2$ (0.2–20 mmol/L). The final value is an average of three measured values. The details of the zeta potential test can be found in the reference [26].

2.4 SEM

The investigation of the morphology of hydration products was carried out using a Phenom ProX electron microscope. The acceleration voltage value was set as 15 kV and a secondary electron (SED) model was selected. The samples were coated with gold before the SEM observations. The details of the SEM test can be found in the reference [27]

2.5 Isothermal calorimetry

The date on cement hydration exothermic rate was obtained by a TAM Air isothermal calorimeter. All material was placed in advance at a temperature of 20 ± 1 °C for 12 h. The MWCNT was sonicated for 15 min using the ultrasonic cleaner. After equilibrating the MWCNT suspension to 20 ± 1 °C, mixing was performed manually for 90 s before sealing the ampoules. The samples were measured in 3 sets for 24 h. The reported data were taken from the average of three replicate specimens.

3 Results and discussion

3.1 Zeta potential

Figure 3 shows the results provided by the experiments on zeta potential measurement. The zeta potentials of limestone powder (LP) and quartz powder (QP) measured by Ouyang et al. [24], and C–S–H tested by Nachbaur [21] and Helene et al. [41] were used for comparison. The increase of the zeta potential is attributed to more Ca^{2+} ions adsorbed on the filler particles' surface with increasing Ca^{2+} concentration. QP and C-S–H particles have a parallel iso-electric point (IEP) at Ca^{2+} concentrations of around 2 mmol/L. LP particles reached the IEP at Ca^{2+} concentrations of approximately 0.4 mmol/L. It indicates the LP particle has a stronger affinity for Ca^{2+} than the QP and C–S–H particle surfaces.

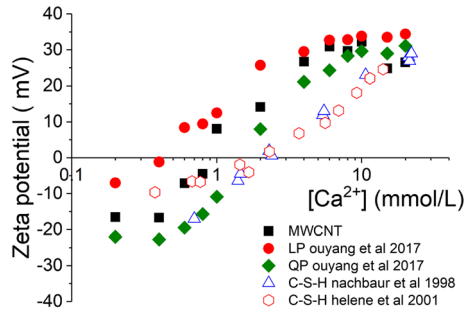

Fig. 3 Development of zeta potential of MWCNT particles in $Ca(OH)_2$ solution

For MWCNT particles, the zeta potential is -16.53 mV at 0.2 mmol/L. Upon the increase of the Ca^{2+} concentration, the absolute value of the zeta potential decreases due to more Ca^{2+} adsorption on the particle's surface. MWCNT particles reach IEP at about 0.9 mmol/L. Then, the high Ca^{2+} concentration exhibited higher zeta potential values up to 6 mmol/L. The maximum zeta potential value (32.2 mV) occurred at 10 mmol/L. The MWCNT potential shows an abnormal decrease at the solution concentration of 15 to 20 mmol/L. This was due to the high $Ca(OH)_2$ concentration, leading to the very high conductivity of the solution. As can be observed, MWCNT has more positive zeta potential than QP and C-S–H particles. These results presented point to the fact that the MWCNT has a strong interaction with Ca^{2+} in cement paste.

3.2 Morphology of hydrates

Figure 4. demonstrates the morphology of hydrates on the cement particles surface in PC and CC paste at 15 min, 1, 4, and 7 h. Figure 4a and b (local enlarged image) show the cement particles' surface in PC paste at 15 min. It can be seen that many granular substances with diameters around 20 nm can be found at the cement surface in PC paste. These substances are likely to be C-S–H nuclei. The morphology of cement surface in CC paste at 15 min is given in Fig. 4c and d (local enlarged image). The granular substances with diameters around 60 nm can be observed at the cement surface in CC paste. The C-S–H particles in CC paste are much larger than those in PC paste. This indicates that the growth of C-S–H is faster in CC paste.

Besides, random MWCNT particles are found on the cement surface in CC paste (Fig. 4d). The diameter of MWCNT is 8–15 nm. The typical diameter of C-S–H particles is 60 nm × 30 nm × 5 nm [23]. In this study, the diameter of MWCNT is smaller than that of C-S–H grains. Meanwhile, no obvious hydration products were found on the surface of MWCNT. It is believed that MWCNT may not be nucleation sites for cement hydration. With a much smaller size, MWCNT cannot offer stable sites for C-S–H nucleation and growth. This will be discussed in more detail in Sect. 3.4.

Figure 4e and f (local enlarged image) demonstrate the morphology of the cement particles in PC paste at 1 h. Granular C–S–H was randomly distributed on the cement particles surface in PC paste with diameters around 20–50 nm. The cement particles surface in CC paste was uniformly covered by the bar-shaped C–S–H with a length of about 130 nm, as shown in Fig. 4g and h (local enlarged image). The C–S–H on cement surface in CC paste has a higher number and larger diameter than that in CC paste.

Figure 4i and j (local enlarged image) illustrate the morphology of cement surface in PC paste at 4 h. It can be seen that the C-S–H is granular and bar-shaped with diameters of about 20–50 nm and bar lengths of about 90 nm. The cement particles surface in PC paste is shown in Fig. 4k and l (partially enlarged images). As can be observed, C–S–H is bar-shaped and overlapped, forming a three-dimensional structure.

Figure 4n and m (local enlarged image) demonstrate the morphology of cement surface in PC paste at 7 h. As can be seen, C–S–H is striped and has a length of about 130 nm. A three-dimensional structure was formed with a large number of granular C–S–H. Whereas, the number of C-S–H grains is much higher than that in PC paste, as shown in Fig. 4o and p (partially enlarged image).

3.3 Cement hydration heat calorimetry analysis

Figure 5a demonstrates the heat flow results, describing the net hydration reaction kinetics of the cement for the first 24 h. Both CC paste and PC paste enter the acceleration phase at approximately 0.40 h. The peak of PC paste appears at 7.81 h. The MWCNT modified cement paste shows a shorter time (7.25 h) to arrive at the peak with a higher accelerating rate and heat flow. The time to reach the peak for CC paste is 7.2% less than that of PC paste. In the heat flow peak, the peak value for CC paste and PC paste is 2.69 and 2.58 mW/g. The peak of heat flow of CC paste is 4.3% higher than that of PC paste. This result shows the presence of MWCNT enhances the hydration reaction compared to the CC paste.

The accumulated hydration heat is showed in Fig. 5b. At a given time, the accumulated heat of hydration of the CC paste was higher than that of the PC paste. At approximately 8.6 h of hydration, the slopes of the two lines are similar. The heat of PC and CC paste is 43.55 and 47.73 J/g at this time. The accumulated hydration heat of CC paste is 9.6% higher than that of PC paste. This result also indicates

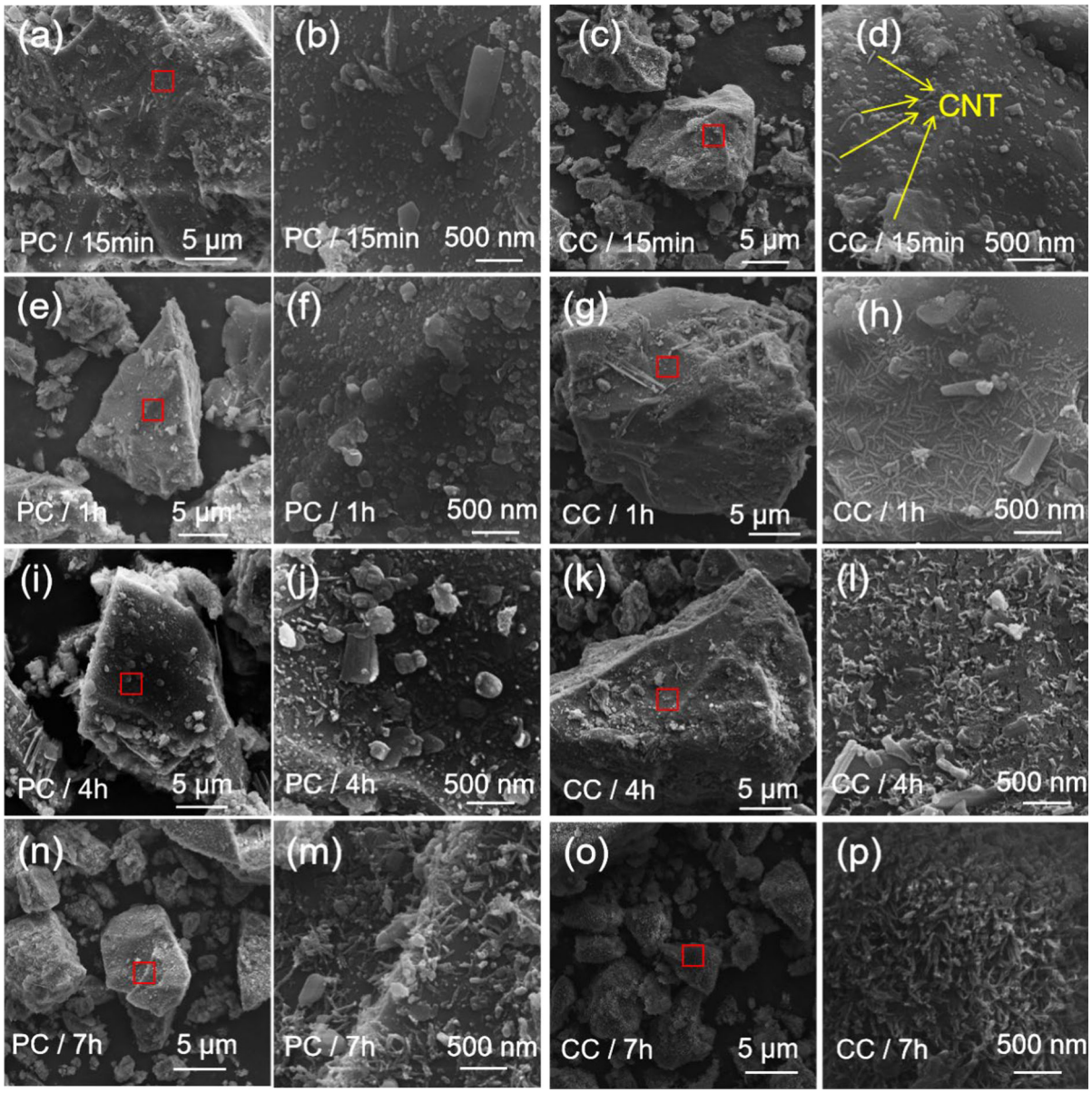

Fig. 4 Morphology of hydrates at cement surfaces in PC paste at 15 min (**a**, **b**), 1 h (**e**, **f**), 4 h (**i**, **j**), and 7 h (**m**, **n**) and in CC paste at 15 min (**c**, **d**), 1 h (**g**, **h**), 4 h (**k**, **l**) and 7 h (**o**, **p**)

that the presence of MWCNT enhances the cement hydration reaction.

3.4 Discussion

As mentioned, there are two processes of the formation of C–S–H: the nucleation process and the nucleation growth process. At the beginning of cement hydration, the ions in the pore solution of cement paste are adsorbed to form ion clusters on the matrix surface. These ionic clusters are unstable and may redissolve into solution before reaching a critical cluster [40]. These stable clusters then form nuclei, which gradually enter the growth process [13]. When MWCNT, cement, and water were mixed, the solution quickly contains multiple ions. The surfaces of MWCNT are soon charged [20, 28]. The counter-ions are absorbed in MWCNT' surfaces, leading to zeta potential

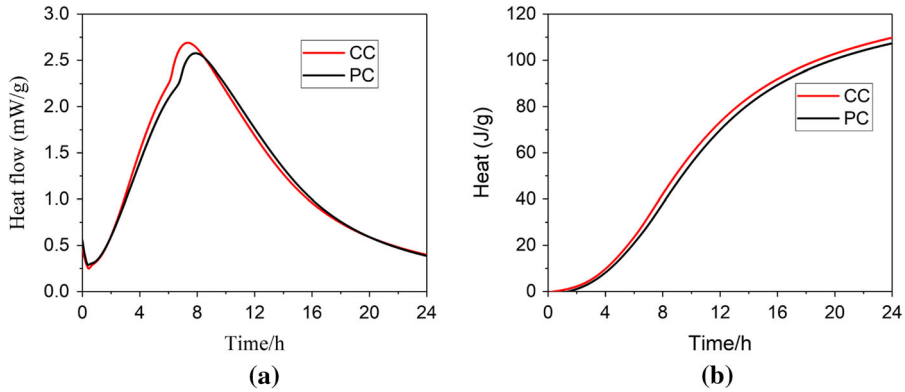

Fig. 5 Rate of hydration heat (**a**) and total accumulated hydration heat (**b**) of CC and PC paste

changed from negative to positive, as shown in Fig. 3. The interaction of the MWCNT surface with Ca^{2+} is stronger than the interaction of QP and C–S–H with Ca^{2+}, resulting in a higher potential for MWCNT than for QP and C–S–H at a given Ca^{2+} concentration. With a strong interaction with Ca^{2+}, MWCNT can significantly improve the migration of ions in cement pore solutions [16], accelerating the formation of 'stable nuclei' and the growth of C–S–H. As a result, a large quantity of C–S–H particles is generated on the cement surface (Fig. 4). The hydration rate of cement mainly depends on the number of C–S–H [30]. Therefore, the CC paste has a faster exothermic rate and a larger exothermic amount of heat than the PC cement paste, as shown in Fig. 5.

It is noted that the diameter of MWCNT is smaller than the diameter of C–S–H, and the ion clusters on the surface of MWCNT would not be stable and grow to a mature nucleus. Therefore, it is doubtful whether MWCNT has a 'nucleation effect' during the cement hydration process. Previous studies [25] have shown that limestone powder (LP) plays a 'nucleation effect' to promote cement hydration. To further investigate the mechanism of MWCNT to promote cement hydration, the morphology of hydrates on the LP surface in cement paste was compared. An LP paste was prepared. The water-cement ratio was 0.4, the LP content was 30% and the cement content was 70%. Figure 6 shows the morphology of hydrates on the cement particles surfaces in PC paste and the cement (CEM) and LP particles surface in LP paste after 4 h of hydration. In the PC paste (Fig. 6a), there are only some small granular C–S–H on the CEM particle's surface. In the LP paste, the morphology of C–S–H on the surface of cement particles is similar to that of the CC paste (Fig. 6b). The LP particles surface is covered with a much more amount of C–S–H (Fig. 6c). C-S–H preferentially nucleates on the LP surface with high density and directional growth, thus facilitating the cement hydration. However, in the cement paste with MWCNT (Fig. 4), the MWCNT surface was not found to have C–S–H and the cement particle surface was covered with more C–S–H. The mechanism of MWCNT promoting cement hydration may be different from the 'nucleation effect' of LP. This indicates that MWCNT may not be the nucleation site for C–S–H. The acceleration of cement hydration caused by the addition of MWCNT could attribute to the high migration of ions derived by MWCNT in cement paste, as illustrated in Fig. 7, rather than the 'nucleation effect'.

4 Conclusions

In this study, zeta potential measurement was performed to characterize the surface charge properties of MWCNT. The morphology of hydrates on cement surface in cement paste with and without MWCNT was observed using SEM. The exothermic evolution of early cement paste was analyzed with isothermal calorimetry. Then, the mechanism of the effect of MWCNT on cement hydration was discussed. The conclusions of this study are as follows:

(1) Compared with QP and C-S-H particles, MWCNT has a more positive zeta potential in $Ca(OH)_2$ solutions, indicating that MWCNT's surface has a higher affinity for Ca^{2+} ions.

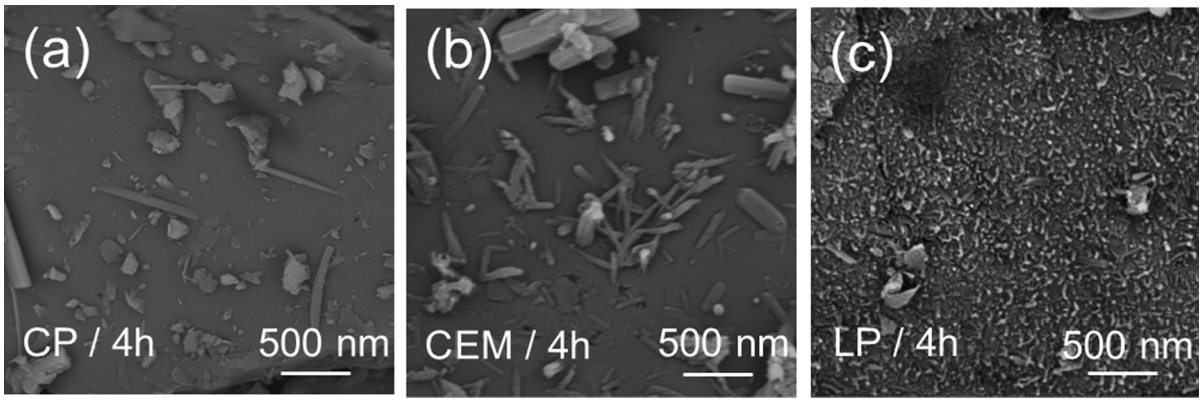

Fig. 6 Morphology of hydrates on cement particles surfaces in PC paste (**a**), CEM (**b**) and LP (**c**) particles surfaces in LP paste at 4 h

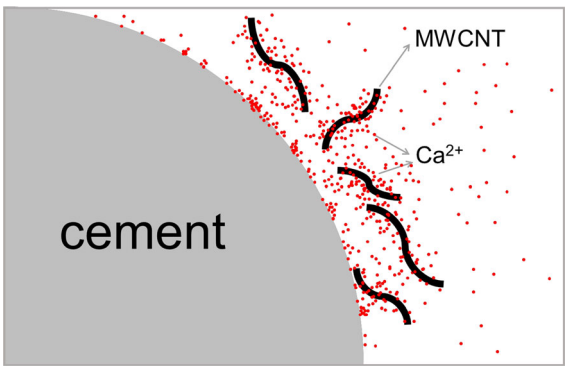

Fig. 7 Schematic diagram of the effect of MWCNT on the interactions of cement surface with Ca^{2+} ions

(2) MWCNT facilitates the nucleation and growth of C-S-H. Compared to PC pastes, the C-S-H size on the cement particle surface of CC pastes is larger and more numerous.
(3) In the CC paste, the appearance of the hydration peak was advanced by 7.2%, while the peak hydration increased by 4.3%. The accumulated hydration heat of CC paste is 9.6% higher than that of PC paste during the first 8.6 h of hydration.
(4) With a strong interaction with Ca^{2+}, MWCNT can significantly improve the migration of ions in cement pore solutions, facilitating the formation of 'stable nuclei' and the growth of C-S-H at the cement surface. The acceleration of cement hydration caused by the addition of MWCNT could attribute to the high migration of ions driven by MWCNT rather than the 'nucleation effect'. Since the diameter of MWCNT is smaller than the diameter of C-S-H, the ion clusters on the surface of MWCNT would not stable and grow to a mature nucleus.

Funding The authors would like to acknowledge the financial support from the National Nature Science Foundation of China (Grant No. 52008119), the Natural Science Foundation of Guangdong Province (Grant No. 2019A1515110799 and 2021A1515012624), and the 111 Project (Grant No. D21021) and the Guangzhou Municipal Science and Technology Project (Grant No. 20212200004).

Declarations

Conflict of interest The authors declare that they have no known competing financial interests or personal relationships that could have appeared to influence the work reported in this paper.

References

1. Dong W, Li W, Luo Z, Guo Y, Wang K (2020) Effect of layer-distributed carbon nanotube (CNT) on mechanical and piezoresistive performance of intelligent cement-based sensor. Nanotechnol 31(50):505503–505516
2. Dong W, Li W, Shen L, Sun Z, Sheng D (2020) Piezoresistivity of smart carbon nanotubes (CNTs) reinforced cementitious composite under integrated cyclic compression and impact. Compos Struct 241:112106–112138
3. Dong W, Li W, Tao Z, Wang K (2019) Piezoresistive properties of cement-based sensors: review and perspective. Constr Build Mater 203:146–163
4. Dong W, Li W, Wang K, Shah SP (2021) Physicochemical and piezoresistive properties of smart cementitious composites with graphene nanoplates and graphite plates. Constr Build Mater 286:122943–122955
5. El-Gamal SMS, El-Hosiny FI, Amin MS, Sayed DG (2017) Ceramic waste as an efficient material for enhancing the fire

resistance and mechanical properties of hardened Portland cement pastes. Constr Build Mater 154:1062–1078
6. Garrault-Gauffinet S, Nonat A (1999) Experimental investigation of calcium silicate hydrate (C-S-H) nucleation. J Cryst Growth 200(3/4):565–574
7. Goldberg S (1992) Chemistry of the solid-water interface: processes at the mineral-water and particle-water interface in natural systems. Geochim Cosmochim Acta 57(3):205–219
8. Han B, Yang Z, Shi X, Yu X (2012) Transport properties of carbon-nanotube/cement composites. J Mater Eng Perform 22(1):184–189
9. Hawreen A, Bogas JA (2018) Influence of carbon nanotubes on steel–concrete bond strength. Mater Struct 51(6):1–10
10. Iqbal S, Ali I, Room S, Khan SA, Ali A (2019) Enhanced mechanical properties of fiber reinforced concrete using closed steel fibers. Mater Struct 52(3):1–10
11. Jang D, Yoon HN, Farooq SZ, Lee HK, Nam IW (2021) Influence of water ingress on the electrical properties and electromechanical sensing capabilities of CNT/cement composites. J Build Eng 42:103065–103075
12. Konsta-Gdoutos MS, Metaxa ZS, Shah SP (2010) Multi-scale mechanical and fracture characteristics and early-age strain capacity of high performance carbon nanotube/cement nanocomposites. Cem Conc Compos 32(2):110–115
13. Krautwurst N, Nicoleau L, Dietzsch M, Lieberwirth I (2018) Two-step nucleation process of calcium silicate hydrate, the nano-brick of cement. Chem Mater 30:2895–2904
14. Leonavičius D, Pundienė I, Girskas G, Pranckevičienė J, Kligys M, Kairytė MA (2018) The effect of multi-walled carbon nanotubes on the rheological properties and hydration process of cement pastes. Constr Build Mater 189:947–954
15. Li F, Liu L, Yang Z, Li S (2021) Influence of modified multi-walled carbon nanotubes on the mechanical behavior and toughening mechanism of an environmentally friendly granulated blast furnace slag-based geopolymer matrix. Ceram Int 47(1):907–922
16. Makar JM, Chan GM (2009) Growth of cement hydration products on single-walled carbon nanotubes. J Am Ceram Soc 92(6):1303–1310
17. Mansouri Sarvandani M, Mahdikhani M, Aghabarati H, Haghparast Fatmehsari M (2021) Effect of functionalized multi-walled carbon nanotubes on mechanical properties and durability of cement mortars. J Build Eng 41:102407–102416
18. Mendoza Reales OA, Dias Toledo Filho R (2017) A review on the chemical, mechanical and microstructural characterization of carbon nanotubes-cement based composites. Constr Build Mater 154:697–710
19. Meng S, Ouyang X, Fu J, Niu Y, Ma Y (2021) The role of graphene/graphene oxide in cement hydration. Nanotechnol Rev 10(1):768–778
20. Moulin F, Devel M, Picaud S (2005) Molecular dynamics simulations of polarizable nanotubes interacting with water. Phys Rev B 71(16):1–7
21. Nachbaur PCNL, Nonat S, Mutin JC (1998) Electrokinetic properties which control the coagulation of silicate cement suspensions during early age hydration. J Coll Interface Sci 202(2):261–268
22. Nalon GH, Lopes Ribeiro JC, Pedroti LG, Duarte de Araújo EN, Franco de Carvalho JM, Soares de Lima GE, De Moura GL (2021) Residual piezoresistive properties of mortars containing carbon nanomaterials exposed to high temperatures. Cem Concr Compos 121:104104–104127
23. Nonat A (2004) The structure and stoichiometry of C-S-H. Cem Concr Res 34(9):1521–1528
24. Ouyang X, Koleva DA, Ye G, Van Breugel K (2017) Insights into the mechanisms of nucleation and growth of C-S–H on fillers. Mater Struct 50(5):1–13
25. Ouyang X, Koleva DA, Ye G, Van Breugel K (2017) Understanding the adhesion mechanisms between C S H and fillers. Cem Concre Res 100:275–283
26. Ouyang X, Wang L, Fu J, Xu S, Ma Y (2021) Surface properties of clay brick powder and its influence on hydration and strength development of cement paste. Constr Build Mater 300:123958–123967
27. Ouyang X, Wang L, Xu S, Ma Y, Ye G (2020) Surface characterization of carbonated recycled concrete fines and its effect on the rheology, hydration and strength development of cement paste. Cem Concr Compos 114:1–10
28. Paillet M, Poncharal P, Zahab A (2005) Electrostatics of individual single-walled carbon nanotubes investigated by electrostatic force microscopy. Phys Rev Lett 94(18):186801–186805
29. Pellenq RJM, Van Damme H (2011) Why does concrete set?: The nature of cohesion forces in hardened cement-based materials. MRS Bull 29(5):319–323
30. Petersson PE (1981) Crack growth and development of fracture zones in plain concrete and similar materials. Report TVBM 1006:1–193
31. Petrunin S, Vaganov V, Reshetniak V, Zakrevskaya L (2015) Influence of carbon nanotubes on the structure formation of cement matrix. IOP Conf Series: Mater Sci Eng 96:1–6
32. Poppe AM, De Schutter G (2005) Cement hydration in the presence of high filler contents. Cem Concre Res 35(12):2290–2299
33. Qin R, Zhou A, Yu Z, Wang Q, Lau D (2021) Role of carbon nanotube in reinforcing cementitious materials: an experimental and coarse-grained molecular dynamics study. Cem Concre Res 147:106517–106529
34. Ren Z, Liu Y, Yuan L, Luan C, Wang J, Cheng X, Zhou Z (2021) Optimizing the content of nano-SiO_2, nano-TiO_2 and nano-$CaCO_3$ in Portland cement paste by response surface methodology. J Build Eng 35:102073–102085
35. Shi T, Gao Y, Corr DJ, Shah SP (2019) FTIR study on early-age hydration of carbon nanotubes-modified cement-based materials. Adv Cem Res 31(8):353–361
36. Siddique R, Mehta A (2014) Effect of carbon nanotubes on properties of cement mortars. Constr Build Mater 50:116–129
37. De Souza TC, Pinto G, Cruz VS, Moura M, Ladeira LO, Calixto JM (2020) Evaluation of the rheological behavior, hydration process, and mechanical strength of Portland cement pastes produced with carbon nanotubes synthesized directly on clinker. Constr Build Mater 248:118686–118699
38. Tafesse M, Kim HK (2019) The role of carbon nanotube on hydration kinetics and shrinkage of cement composite. Compos Part B: Eng 169:55–64

39. Tafesse M, Lee NK, Alemu AS, Lee HK, Kim SW, Kim HK (2021) Flowability and electrical properties of cement composites with mechanical dispersion of carbon nanotube. Constr Build Mater 293:123436–123454
40. Vekilov PG (2010) Nucleation. Cryst Growth Des 10(12):5007–5019
41. Viallis-Terrisse H, Nonat A, Petit JC (2001) Zeta-potential study of calcium silicate hydrates interacting with alkaline cations. J Colloid Interface Sci 244(1):58–65
42. Wang J, Han B, Li Z, Yu X, Dong X (2019) Effect investigation of nanofillers on C-S-H gel structure with Si NMR. J Mater Civil Eng 31(1):04018352–04018364
43. Xu S, Lyu Y, Xu S, Li Q (2019) Enhancing the initial cracking fracture toughness of steel-polyvinyl alcohol hybrid fibers ultra high toughness cementitious composites by incorporating multi-walled carbon nanotubes. Constr Build Mater 195:269–282
44. Zhao L, Guo X, Song L, Song Y, Dai G, Liu J (2020) An intensive review on the role of graphene oxide in cement-based materials. Constr Build Mater 241:117939–117956